JOURNAL OF PROPULSION AND POWER
Vol. 14, No. 6, November–December 1998

Mixer–Ejector Noise-Suppressor Model

David E. Tew,* Brian S. Teeple,† and Ian A. Waitz‡
Massachusetts Institute of Technology, Cambridge, Massachusetts 02139

A flexible and efficient compressible mixer–ejector model is described. This model is used to predict the performance of ejectors employing lobed mixers. Through comparisons with experimental data, the model is shown to qualitatively capture the impact of streamwise vorticity on the evolution of the mixing layer and to quantitatively predict the change in the pressure coefficient through the duct associated with the mixing process to within 15%. The relative accuracy, speed, and flexibility of the model make it useful as a preliminary design tool. Two design trade studies are performed with the model. First, the model is used to assess the impact of streamwise vorticity on the thrust and pumping performance of a supersonic–subsonic mixer–ejector; for the mixer geometry utilized in this study, pumping and thrust augmentations are associated with the addition of streamwise vorticity. Second, the impact of mixer height on the effectiveness of streamwise vorticity is evaluated. The results of this study demonstrate that the effectiveness of streamwise vorticity decreases with increasing lobe height-to-wavelength ratio, and for the higher height-to-wavelength ratios investigated, a net performance penalty is associated with the addition of streamwise vorticity.

Nomenclature

A_{exit}/A_{in} = duct exit/inflow area ratio
A_s/A_p = secondary to primary inflow area ratio
A_{wet}/A_{in} = mixer wetted to inflow area ratio
C_D = mixer drag coefficient
C_f = skin friction coefficient
Cp_{super} = supersonic pressure coefficient
C_{TG} = gross thrust coefficient
h^* = lobe height in wavelengths
L^*_{eff} = effective interface length in wavelengths
M_p = primary Mach number
M_s = secondary Mach number
M_{sc} = scalar mixedness
Pt_p = primary stream total pressure
$p_{p|_{LE}}$ = primary stream inflow static pressure
Re_Γ = circulation Reynold's number, Γ/ν_t
Tt_s/Tt_p = secondary/primary total temperature ratio
t^* = nondimensional time
v^* = nondimensional complex vortex velocity
x^* = distance from the trailing edge in wavelengths
α = lobe half-angle
Γ^* = nondimensional streamwise circulation
γ^* = nondimensional streamwise circulation about an individual vortex normalized by total circulation
δ'_{vel} = growth rate of velocity thickness of planar shear layer
ε = initial boundary-layer thickness in wavelengths
ζ^* = nondimensional complex vortex position
λ = lobe peak-to-peak wavelength
ν_t = turbulent viscosity
φ = normalized static pressure

Received May 19, 1997; revision received March 14, 1998; accepted for publication March 15, 1998.

*Postdoctoral Associate, Aero-Environmental Research Laboratory, Department of Aeronautics and Astronautics; currently Associate Research Engineer, United Technologies Research Center, M/S 29, 411 Silver Lane, East Hartford, CT 06108. E-mail: davetew@alum.mit.edu. Member AIAA.

†Graduate Research Assistant, Aero-Environmental Research Laboratory, Department of Aeronautics and Astronautics, Room 31-231. E-mail: bsteeple@mit.edu.

‡Associate Professor of Aeronautics and Astronautics, Aero-Environmental Research Laboratory, Room 31-266. E-mail: iaw@mit.edu. Senior Member AIAA.

I. Introduction

A TYPICAL mixer–ejector noise suppressor is depicted in Fig. 1. These suppressors entrain cold secondary air into a duct and mix that air with a hot, fast primary stream. This mixed stream then leaves the duct at a lower velocity than that of the primary. The reduction in jet velocity decreases the intensity of the turbulent mixing process between the exhaust jet and ambient air and thereby reduces the radiated noise. In an effort to augment the mixing rate of the primary and secondary streams and, hence, minimize the required length of the ejector duct, lobed mixers are typically employed to enhance the mixing rate between the two streams. These mixers augment mixing by both increasing the initial interface length between the streams and by introducing streamwise vorticity into the mixing layer.[1–4]

The mixer–ejector noise suppressor model presented in this paper was developed to make rapid ejector performance predictions to enable mixer–ejector optimization and design trade studies. For such studies it is often desirable to conduct a large number of simulations over a wide range of design parameters. Hence, computational efficiency is of prime concern. Thus, the approach taken was to model only the physical processes necessary to make useful performance predictions.

The resulting model is used to calculate the pumping and thrust of a mixer–ejector given the mixer lobe and ejector duct geometries and operating conditions. Additionally, the model also provides the local quasi-one-dimensional flow conditions through the duct, including the local mixedness, static pressure, and entropy. It is distinguished from many other simplified ejector design tools in that it includes a higher-fidelity numerical simulation that links the mixing process within the duct to details of the mixer lobe geometry.

A description of the model is presented in Sec. II. In Sec. III, model predictions are compared to experimental data; these data include Mie images and mixing duct wall static pressure measurements. In Sec. IV the model is used to assess the impact of streamwise vorticity on the thrust and pumping performance of supersonic–subsonic ejectors, and in Sec. V the model is further utilized to assess the impact of the mixer

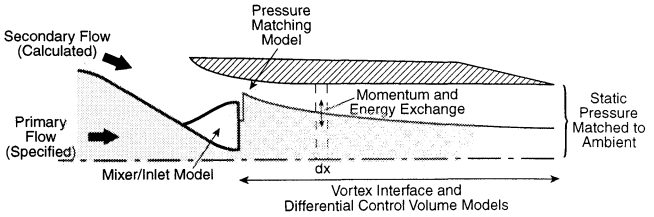

Fig. 1 Ejector model schematic.

height-to-wavelength ratio h^* on the effectiveness of streamwise vorticity. The work is then summarized, and conclusions are presented in Sec. VI.

II. Description of the Mixer–Ejector Model

The mixer–ejector model consists of a series of quasi-one-dimensional control volume analyses and a vortex dynamics code. Each of these components is briefly described next; more detailed descriptions follow in Secs. II.A–II.D. A schematic of a mixer–ejector is drawn in Fig. 1 with the locations of the different component models indicated.

1) Mixer/inlet: Given the mixer geometry and the inflow conditions, a series of two integral control volumes over the mixer are used to first calculate the form drag coefficient and then to calculate the mixer trailing-edge conditions from the inflow conditions and total drag coefficient.

2) Pressure matching: At the trailing edge of the mixer, the static pressures in the supersonic primary and subsonic secondary streams may not be matched. Hence, a two-stream control volume is used to model the expansion/compression of the two streams that occurs as the pressures are matched.

3) Vortex interface: Downstream of the pressure-matched point, a discrete vortex interface model is used to calculate the local interface length between the two streams.

4) Differential control volume: Given the pressure-matched flow conditions from the matching calculation and the interface length distribution from the vortex code, the differential conservation equations are integrated from the pressure-matched point at the mixer trailing edge to the duct exit. In the integration the local rate of transport of momentum and energy between the mixing streams is assumed to be proportional to the local interface length and the local turbulent viscosity.

When the four components are combined into the full mixer–ejector model, the secondary mass flow is iterated on to match the duct exit static pressure to ambient.

A. Mixer/Inlet Model

Given the mixer lobe angle α, the lobe height-to-wavelength ratio h^*, the lobe height-to-duct height ratio (penetration), and inflow conditions, the mixer model is used to calculate the shed streamwise circulation and the trailing-edge mass-averaged flow conditions for each stream.

The shed streamwise circulation is calculated using the scaling law developed by Barber et al.[5] For the square lobe geometries investigated in this work

$$\Gamma^* = \Gamma/\bar{U}h = 2 \tan \alpha \tag{1}$$

Barber et al.[5] and O'Sullivan et al.[6] demonstrated that for lobes with half-angles α less than 22 deg, the circulation predicted by the scaling law in Eq. (1) is within 5% of values calculated in numerical simulations of the lobe flow.[1] Additionally, for square lobe mixers, the strength of the vorticity distribution is assumed constant along the vertical sidewalls of the mixers. For more complicated mixer geometries, panel method, Euler, or Navier–Stokes computations over the lobes may be required to establish the lobe trailing-edge vorticity distribution.

Although streamwise vorticity is often introduced to enhance ejector performance by further augmenting the mixing rate between the primary and secondary streams, total pressure losses are also associated with the vectoring of the flow off-axis to generate the vorticity. Indeed, the net impact of streamwise vorticity on ejector thrust performance is a balance between the increased thrust associated with increased mixing rates and the decreased thrust associated with its generation. In Sec. V.B the trade between these two effects is illustrated.

The loss penalty for introducing streamwise vorticity is assessed in the mixer model. The approach taken is to assume that the flow that has been vectored off-axis over the mixer is turned nonisentropically back into the axial direction in the mixing duct. Hence, the trailing-edge crossflow kinetic energy is discarded. This is a worst-case scenario, as some of the flow may be isentropically turned back into the axial direction.

The total mixer drag coefficient is calculated in two steps. First, a form drag coefficient is calculated from an isentropic, constant area control volume over the mixer. In this control volume, it is assumed that the flow in the lobe troughs leaves at the mixer metal angle and the flow outside the troughs leaves in the axial direction. Hence, the analysis is not valid if the flow has separated from the mixer. Furthermore, the static pressure is assumed to be constant in the trailing-edge plane.

Second, the form drag coefficients for each stream are then used in a nonisentropic mixer control volume from which the one-dimensional trailing-edge conditions are calculated. In this control volume the conservation of mass, momentum, and energy are solved for the mixer trailing-edge conditions given the inflow conditions and the total mixer drag coefficient. The total mixer drag coefficient includes both the form and skin friction components

$$C_D = C_{D|_{\text{skin}}} + C_{D|_{\text{form}}} \tag{2}$$

The skin friction drag is calculated from

$$C_{D|_{\text{skin}}} = C_f(A_{\text{wet}}/A_{\text{in}}) \tag{3}$$

where A_{wet} is the wetted area of the primary stream side of the mixer. This analysis is performed in two steps so that the system of equations used to calculate the form drag may be closed by assuming the mixer flow is isentropic. Hence, the mixer skin friction is assumed to have no impact on the mixer form drag.

In Fig. 2, the skin friction, form, and total mixer drag coefficients are plotted for a range of forced mixer geometries. For the sake of clarity, only the primary stream coefficients

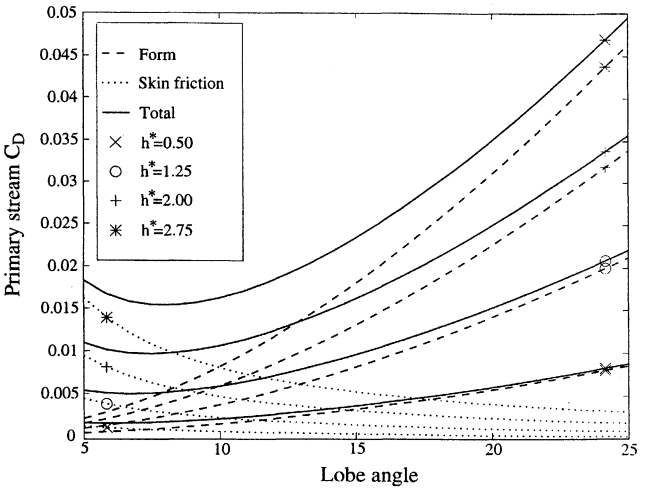

Fig. 2 Forced mixer drag coefficients as a function of lobe angle and lobe height-to-wavelength ratio. Skin friction coefficient: $C_f \approx 0.003$.

are plotted for four different mixer h^*, for lobe half-angles ranging from 5 to 25 deg, at a primary Mach number of 1.6 and a C_f of 0.003. This C_f was determined from the experiments described in Sec. III. For this analysis, the duct geometry was held constant; hence, as the mixer height increases, the fraction of the duct inflow that passes through the mixer increases. In this comparison, as the mixer height increases from 0.5 to 2.75, the fraction of the duct into which the lobe penetrates increases from 0.1 to 0.55.

For lobe angles between 5 and 25 deg, $C_{D|_{\text{form}}}$ is the largest contributor to the mixer drag; as the lobe angle increases, the relative importance of the form drag increases. The opposing trends in $C_{D|_{\text{form}}}$ and $C_{D|_{\text{skin}}}$ with varying lobe angles results in a minimum in the C_D vs α curve. For all the mixers this minimum occurs at $\alpha \approx 7$ deg; however, the lobe angle for minimum drag increases slightly with increasing mixer height.

B. Pressure Matching

For the supersonic–subsonic mixer–ejector noise suppressors of interest in this work, the static pressures of the secondary and primary streams at the trailing edge of the mixer may not be matched. If the pressures are indeed not matched, expansion or compression of the two streams will occur.

A two-stream, quasi-one-dimensional model of the pressure-matching process was developed. In the model the inflow conditions are specified based on the mixer/inlet analysis described in Sec. II.A. Furthermore, the subsonic stream is assumed to be isentropic and the static pressures of the two streams are matched at the exit. Additionally, the pressure matching process is assumed to occur in a constant area duct, and in the full mixer–ejector model the pressure-matching region is assumed to be infinitesimally thin. The mixing process then commences immediately downstream of the pressure-matched point. In real mixing layers, the pressure-matching process occurs over a finite region while the two streams are mixing. The approach taken in this analysis is equivalent to assuming that the mixing rate between the two streams does not vary through the pressure-matching region. This approximation is reasonable for static pressure ratios not far from 1.

The pressure-matched conditions serve as the initial conditions for the differential control volume. Additionally, the matched conditions are used to determine the local growth rate of the shear layer between the streams in the vortex interface model that is described in the next section.

C. Vortex Interface

Given the matched-point flow conditions as well as the total shed streamwise circulation and the vorticity distribution, a discrete vortex simulation is used to calculate the effective interface length L_{eff} between the mixing secondary and primary streams. This effective interface length is then used in the differential control volume to calculate the local rate of transport of momentum and energy.

The discrete vortex simulation uses a series of viscous point vortices to model the cross-stream velocity field downstream of the mixer. A slender body approximation is made in which a steady three-dimensional flowfield is approximated by an unsteady two-dimensional flow.[1,3] In this approximation, time in the unsteady two-dimensional flow corresponds to distance from the trailing edge divided by the mean axial velocity. Such an approximation is only strictly valid for low circulation and small velocity and density differences between the streams. Nonetheless, experiments and numerical simulations have demonstrated that this approximation is useful over a wider range of conditions, inclusive of those investigated in the current study.[1]

A series of vortices are initially positioned to approximate the streamwise vorticity distribution shed by the lobed mixer. The interface between the streams is the curve connecting these vortices. This interface evolves with distance from the trailing edge as the vortices are convected in the induced velocity field. The velocity of the kth vortex at nondimensional time $t^* = x^*\Gamma^*h^*$ is given by

$$\nu_k^* = \left(\frac{i}{2\pi}\right)\sum_{j=1}^{N}\gamma_j^*\frac{\zeta_k^* - \zeta_j^*}{|\zeta_k^* - \zeta_j^*|^2}\left[1 - \exp\left(\frac{-Re_\Gamma}{2t^*}|\zeta_k^* - \zeta_j^*|^2\right)\right] \tag{4}$$

The rate of diffusion of vorticity is set by Re_Γ, which is a function of the stream-to-stream velocity and density ratios and the convective Mach number per the shear-layer growth rate scaling law developed by Papamoschou and Roshko.[7]

In the calculation of the individual vortex velocities, the velocity fields of a number of viscous vortices are superimposed. This superposition as well is not strictly valid. To assess this approximation, several comparisons were made to simulations performed with a two-dimensional, unsteady Navier–Stokes solver developed by Qiu.[3] Over the range of circulations investigated ($\Gamma^* < 0.5$), the discrete vortex analysis captured the mean rate of decay of streamwise circulation within 10%; this level of agreement suggests that the discrete vortex simulation of the mixing process is indeed a useful approximation for lobed mixer calculations. (Comparisons between the vortex simulation and experimental data are presented in Sec. III.B.) In the discrete vortex analysis, a passive scalar is also tracked to calculate the scalar mixedness and the effective interface length for the calculation of the local rate of transport of momentum and energy in the differential control volume.

In Fig. 3, the predicted vortex paths from $x^* = 0$ to 2λ and the fully mixed scalar field at 2λ downstream of a forced mixer are drawn. In each of the plots the curve connecting the vortices is also drawn. The evolution of the cross-stream interface and the growth of the shear layer on that interface as illustrated in Fig. 3 are typical of streamwise vorticity-enhanced mixing layers. The predicted axial scalar mixedness distributions downstream of four mixers are plotted in Fig. 4. The mixers have varying levels of streamwise circulation. The trends in mixing rate observed are also typical of those observed in previous experimental and computational studies of streamwise vorticity-enhanced mixing layers.[1–3,6,8] (A more detailed comparison with experimental data will be presented in Sec. III.B.)

From scalar mixedness distributions such as those shown in Fig. 4, the local effective interface length for transport of momentum and energy between the streams is then calculated

$$L_{\text{eff}}^* = \frac{\dfrac{\partial M_{\text{sc}}}{\partial x^*}}{\left.\dfrac{\partial M_{\text{sc}}}{\partial x^*}\right|_{\text{FP}}} \tag{5}$$

$\partial M_{\text{sc}}/\partial x^*$ is the local scalar mixing rate downstream of the mixer of interest, and $\partial M_{\text{sc}}/\partial x^*|_{\text{FP}}$ is the scalar mixing rate

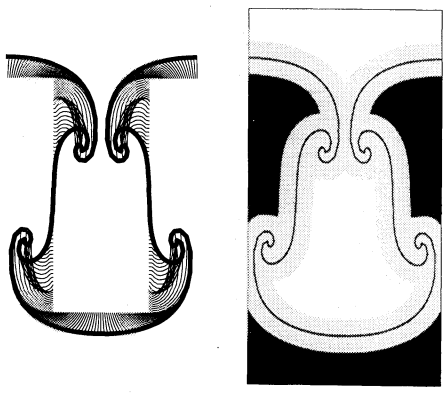

Fig. 3 Vortex paths from 0 to 2λ and scalar field at 2λ for $\Gamma^* = 0.5$, $\delta'_{\text{vel}} = 0.10$, and $\varepsilon^* = 0.25$.

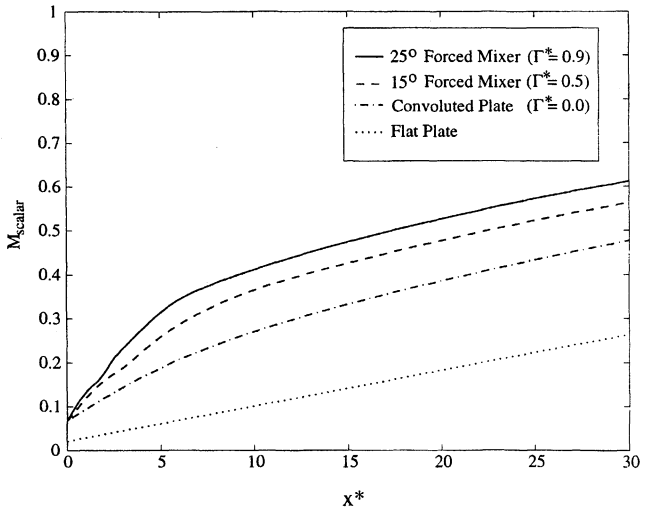

Fig. 4 Modeled axial scalar mixedness distribution downstream of the four mixers investigated experimentally in Ref. 10 with $\delta'_{vel} = 0.10$, and $\varepsilon^* = 0.25$ ($h^* = 1.25$).

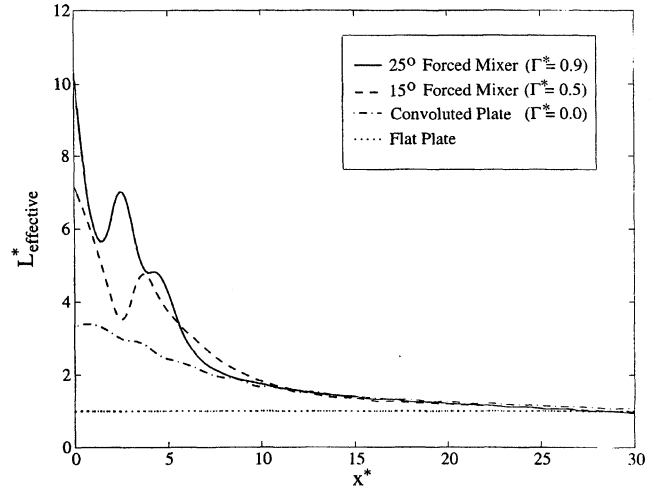

Fig. 5 Modeled effective interface length distribution downstream of the four mixers investigated experimentally in Ref. 10 with $\delta'_{vel} = 0.10$, and $\varepsilon^* = 0.25$ ($h^* = 1.25$).

downstream of the flat plate mixer at the same inflow conditions. The L^*_{eff} distributions calculated from Eq. (5) and the scalar mixedness distributions in Fig. 4 are plotted in Fig. 5. In these L^*_{eff} distributions, the two mixing enhancement mechanisms associated with lobed mixers may be identified. First, an increased mean L^*_{eff} results from the increased initial interface length offered by lobed mixers ($\Gamma^* = 0.01$ case). Second, an additional increase in the mean L^*_{eff} downstream of the trailing edge is associated with the introduction of streamwise vorticity.

D. Differential Control Volume

Given the matched-point flow conditions calculated in the static pressure matching control volume and the effective interface length distribution from the discrete vortex interface analysis, a two-stream differential control volume is used to calculate the axial distribution of the one-dimensional flow quantities throughout the ejector duct.

In this control-volume analysis, the two coflowing streams interact via the exchange of momentum and energy.[9] The local rate at which transport occurs between the two streams is calculated using the local effective interface length and local planar shear-layer growth rate. The mass, momentum, and energy conservation equations for each stream are then integrated from the pressure-matched point to the duct exit assuming that the static pressure is constant in an axial plane. Hence, the axial distributions of the one-dimensional flow conditions are determined through the duct.

E. Complete Mixer–Ejector Model

When the complete model is utilized as an ejector performance estimation tool, the primary (NPR) and secondary (SNPR) stream nozzle pressure ratios, the primary to secondary total temperature ratio Tt_p/Tt_s, the primary Mach number M_p, and the mixer and duct geometries are specified. The secondary inflow Mach number, or secondary mass flow, is then iterated upon until the predicted duct exit to ambient static pressure ratio is one. The complete mixer–ejector model can be run on an IBM RS6000 workstation in several minutes, and no gridding is required.

III. Assessment of the Model

To assess the full mixer–ejector system model and its components, several comparisons were made to experimental data. These data include Mie images and secondary wall static pressures. The measurements were taken in a series of experiments conducted at United Technologies Research Center.[10,11] These experiments were designed to delineate the impact of streamwise vorticity on compressible mixing layers.

To make this assessment, four different mixers were evaluated–three lobed mixers and one flat plate. The three lobed mixers all had the same trailing-edge shape. They were of square lobe design and had a height-to-wavelength ratio of 1.25. Schematics of the mixers are shown in Fig. 6. Two of the lobed mixers were forced mixers and were designed to shed streamwise circulation; the third mixer was a convoluted plate that shed little streamwise circulation. The lobe exit angles, estimated nondimensional streamwise circulations Γ^*, and designations of three lobed mixers are listed in Table 1.

The circulations shed by the two lobed mixers were estimated using the scaling law given by Eq. (1). The circulation shed by the convoluted plate was estimated from Navier–Stokes computations performed by O'Sullivan[7] on mixer geometries similar to those investigated in the current work.

A. Assessment of Pressure-Matching Analysis

Given the trailing-edge conditions, the pressure-matching control volume was used to calculate the conditions at the pressure-matched point in situations where the primary and secondary trailing-edge static pressures are unmatched. In Fig. 7 the measured supersonic pressure coefficient Cp_{super} at the first wall static pressure tap downstream of the mixers $x^* \approx 0.5$ is plotted along with the calculated Cp_{super} at the predicted pressure matched point for a range of inflow static pressure ratios. Here, the supersonic pressure coefficient at a particular axial location x^* in the duct is defined by Eq. (6):

$$Cp_{super} = \frac{p(x^*) - p_{p|_{LE}}}{Pt_p - p_{p|_{LE}}} \tag{6}$$

For the comparisons shown in Fig. 7, the model predicts the measured pressure coefficient within the uncertainty of the data for secondary to primary static pressure ratios less than 1.2. For static pressure ratios greater than 1.2, the model overpredicts the static pressure rise by as much as 5% of the full range of Cp_{super} variation. This overprediction may be the result of separations moving into the mixers and eventually into the nozzle. Model/data comparisons were also performed at inflow Mach numbers of 1.3 and 2.4; similar agreement between the model and data was observed.[10]

B. Assessment of Discrete Vortex Interface Analysis

Given the matched-point conditions and the shed streamwise vorticity distribution, the discrete vortex interface analysis was

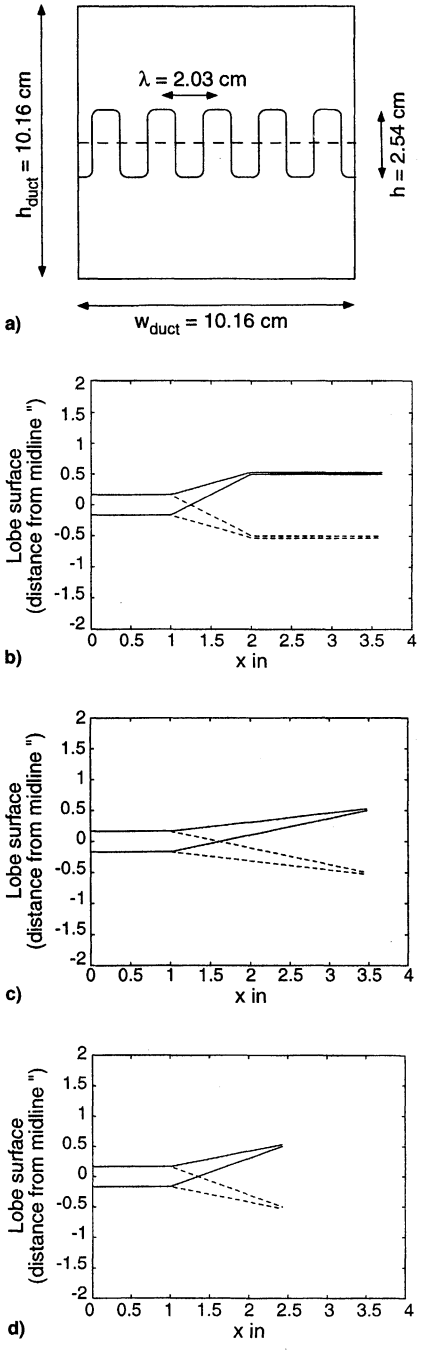

Fig. 6 Lobed mixers evaluated experimentally in Ref. 10: a) Trailing-edge view of all mixers, b) side view of convoluted plate mixer, c) side view of 15-deg forced mixer, and d) side view of 25-deg forced mixer.

used to calculate the scalar field, scalar mixedness, and the effective interface length as a function of distance through the duct for the various mixers evaluated experimentally.

In Fig. 8, experimental time-mean Mie images and calculated fully mixed scalar fields are shown 1, 2, and 3 wavelengths downstream of a 15-deg forced mixer at flow conditions for which the predicted growth rate of the shear layer between the two streams was 0.02 (M_p = 2.4 and M_s = 1.2).

The experimental images were obtained by seeding the high-speed stream with liquid methanol upstream of the plenum chamber. The methanol evaporates and then recondenses through the converging–diverging nozzle. When a laser sheet is passed through the test section, the supersonic stream is illuminated. The images presented in Fig. 8 represent averages of >1800 individual laser pulses. In these images, the illuminated supersonic stream appears white; the subsonic stream appears black; and the mixing layer between them appears gray.

Table 1 Experimental lobed mixer designations, lobe angles, and nondimensional streamwise circulations

Mixer	Angle, deg	Γ*
CP	0	0.03
15 deg FM	15	0.5
25 deg FM	25	0.9

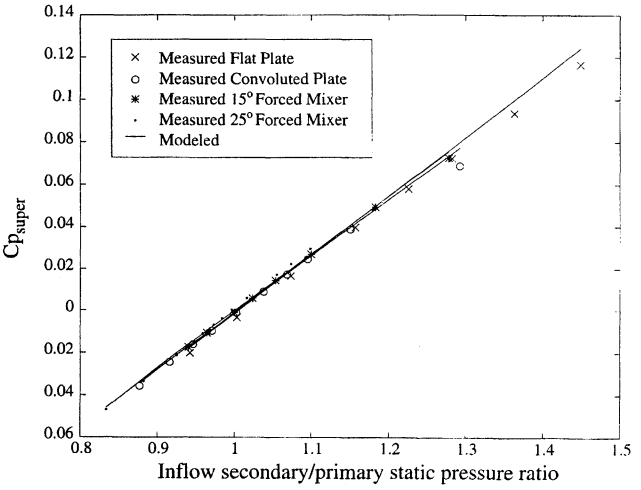

Fig. 7 Comparison between modeled matched-point Cp_{super} and the measured Cp_{super} at the first pressure tap downstream of the trailing edge of each of the mixers. M_p = 1.6. (Error bars on the experimental measurements are smaller than the symbols.)

The intensity-scale in the calculated scalar fields in Fig. 8 is similar to that used for the experimental data. The high-speed stream is white; the low-speed stream is black; and the fully-mixed shear layer is shown in gray. Comparing the experimental images with the simulations, the discrete vortex calculation is seen to qualitatively capture the evolution of the interface with distance from the mixer trailing edge. (A quantitative comparison is made in Sec. III.C.)

Additionally, in Fig. 9 experimental time-mean Mie images and scalar fields are shown again downstream of the 15-deg forced mixer; however, for this case the flow conditions were such that the growth rate of the shear layer was five times that of the case presented in Fig. 8 (M_p = 1.6 and M_s = 0.3). The interface calculation again qualitatively captures the evolution of the interface with distance from the mixer trailing edge.

Also of note in comparing the Mie images and scalar fields in Fig. 8 to those in Fig. 9 is the large difference in the structure of the mixing layers at the same locations downstream of the 15-deg forced mixer, for the two different planar shear-layer growth rates. At the lower shear-layer growth rate, the streamwise vorticity is more effective in stretching the interface downstream of the trailing edge. This point is illustrated in Fig. 10, where the calculated mean effective interface lengths in the mixing duct are plotted vs the planar shear-layer growth rate. (Recall, the rate of transport of momentum and energy in the differential control volume is proportional to L_{eff}.) The mean L_{eff} is plotted for three mixers with the same trailing-edge shape, but shedding different levels of streamwise circulation. At the highest planar shear-layer growth rates, the streamwise vorticity has little impact on L_{eff}. However, at the lowest shear-layer growth rates, the mean L_{eff} downstream of the mixer shedding the highest circulation is three times that of the mixer shedding the least circulation.

The reason for the decreasing impact of streamwise circulation with increasing shear-layer growth rates lies with the

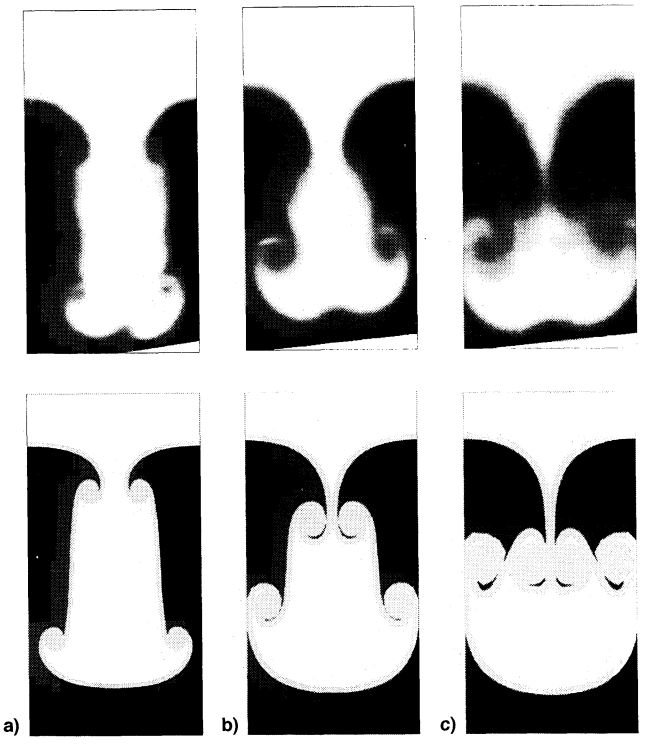

Fig. 8 Vortex model and Mie data crossflow interface structure comparison. Crossflow planes are 1λ, 2λ, and 3λ downstream of the 15-deg forced mixer with M_p = 2.4 and M_s = 1.6. Model parameters: Γ^* = 0.5, δ'_{vel} = 0.02, and ε^* = 0.05: a) Mie: x^* = 1 (model: x^* = 1), b) Mie: x^* = 2 (model: x^* = 2), and c) Mie: x^* = 3 (model: x^* = 3).

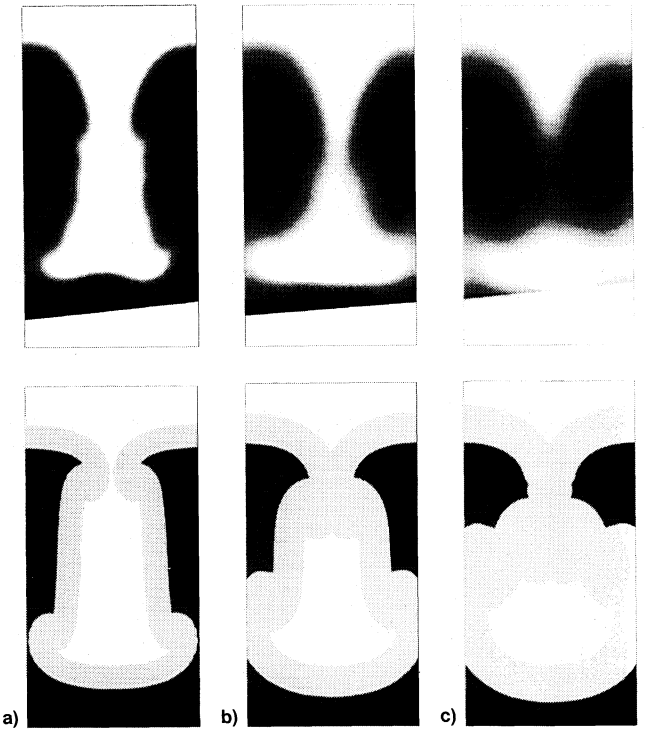

Fig. 9 Vortex model and Mie data crossflow interface structure comparison. Crossflow planes are 1λ, 2λ, and 3λ downstream of the 15-deg forced mixer with M_p = 1.6 and M_s = 0.3. Model parameters: Γ^* = 0.5, δ'_{vel} = 0.10, and ε^* = 0.25: a) Mie: x^* = 1 (model: x^* = 1), b) Mie: x^* = 2 (model: x^* = 2), and c) Mie: x^* = 3 (model: x^* = 3).

increasing rate of the diffusion of the streamwise vorticity away from the interface. For cases with higher shear-layer growth rates, the streamwise vorticity diffuses away from a given interface more rapidly; the strength of the vorticity is reduced through interaction with vorticity of opposite sign shed by adjacent lobe walls. Thus, the streamwise circulation has less distance over which to stretch the interface between the streams.

In summary, the discrete vortex simulation of the flowfield downstream of the 15-deg forced mixer has been shown to qualitatively capture the evolution of the mixing layer as observed in experimental Mie images. Furthermore, the simulations reproduce the experimental observation that the impact of streamwise vorticity on the mixing rate decreases with increasing planar shear-layer growth rate.

C. Assessment of the Mixer–Ejector Model

To quantitatively evaluate the ability of the model to predict the performance of mixer–ejectors, comparisons were made between the modeled and measured duct exit supersonic pressure coefficient (Cp_{super}). In Fig. 11 the duct exit Cp_{super} is plotted vs the pumping at a primary inflow Mach number of 1.6, for three of the mixers evaluated experimentally.[10] In this comparison the primary mass flow is held constant and the secondary mass flow is controlled to vary the pumping. In Fig. 11, the model captures the increasing Cp_{super} with increasing pumping. Furthermore, the model captures the increased pressure rise associated with the mixing augmentation due to the increased initial interface length of the convoluted plate and the additional rise resulting from the mixing augmentation associated with the streamwise vorticity of the forced mixer. In particular, the Cp_{super} change through the duct is captured to within 15% over the experimentally measured range. Similar agreement between the model and data was obtained at primary Mach numbers of 1.3 and 2.4 as well as in situations where both inflow streams were subsonic.[10]

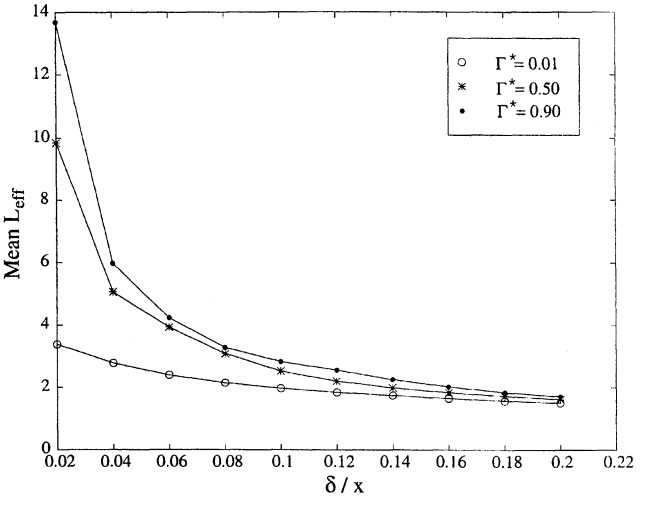

Fig. 10 Mean effective interface length vs planar shear-layer growth rate.

IV. Impact of Streamwise Vorticity on Ejector Performance

To illustrate the utility of the mixer–ejector system model, a design study was conducted to assess the impact of mixer-generated streamwise vorticity on ejector performance. In Fig. 12 the results of a sample sensitivity study conducted with the model are presented. In this study the sensitivity of the ejector performance to the primary nozzle pressure ratio was evaluated for three different mixers: 1) a flat plate, 2) a lobed mixer with a square trailing-edge shape and h^* = 1.25 that shed no streamwise circulation (Γ^* = 0.0), and 3) a forced mixer of the same trailing-edge shape that shed a circulation of Γ^* = 0.5. The

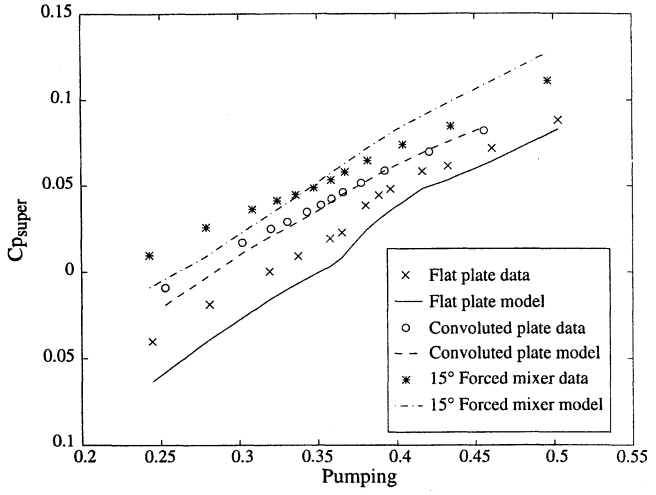

Fig. 11 Full model/data Cp_{super} comparison at duct exit ($x^* = 30\lambda$).

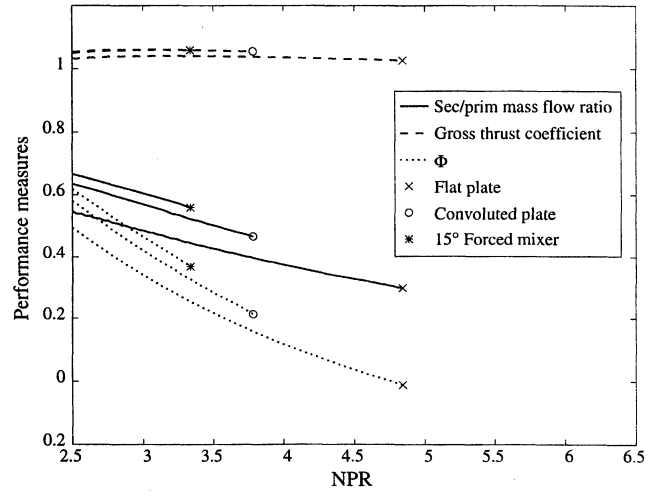

Fig. 12 Predicted pumping and gross thrust coefficient vs NPR. SNPR = 1.0, M_p = 1.6, A_s/A_p = 1.0, and Tt_p/Tt_s = 3.0.

mixer ducts utilized were assumed frictionless; they were five lobe wavelengths in height and 30 lobe wavelengths in length.

Three performance quantities are plotted in Fig. 12, pumping, gross thrust coefficient C_{TG}, and the normalized static pressure ϕ at the duct exit. The pumping is defined as the secondary to primary mass flow ratio. The gross thrust coefficient is the ratio of the mixer–ejector system thrust to the thrust that could be obtained if the primary stream was isentropically expanded to ambient

$$C_{TG} = \frac{\int_{\text{exit}} U\, d\dot{m} - \int_{\text{secondary entrance}} U\, d\dot{m}}{\int_{\text{ideal primary}} U\, d\dot{m}} \tag{7}$$

If $C_{TG} > 1$, a thrust augmentation is associated with the presence of the ejector; if $C_{TG} < 1$, a thrust penalty is associated with the presence of the ejector. The normalized static pressure varies between 0 at the unmixed trailing edge and 1 at the fully mixed conditions

$$\phi(x^*) = \frac{p(x^*) = -p_{p|_{LE}}}{p_{\text{mixed}} - p_{p|_{LE}}} \tag{8}$$

Hence, if $\phi < 1$, the two streams are not fully mixed at the duct exit and additional mixing could be achieved by lengthening the duct.

For this study M_p = 1.6, SNPR = 1, and Tt_p/Tt_s = 3; additionally, the mixer and duct skin friction coefficients were 0. The primary nozzle pressure ratio was varied between 2.5 and the value at which each of the mixer/duct combinations compound choked at the inlet.

For the primary nozzle and duct geometries utilized in this study, at NPR = 2.5, the primary stream was overexpanded relative to the secondary stream at the trailing edge of the mixer. As NPR was increased, the secondary-to-primary static pressure ratio decreased, and the secondary Mach number increased as more secondary fluid was drawn into the ejector. However, the amount of secondary fluid entrained into the ejector was limited by the compound choking of the duct in the pressure matching region. In Fig. 12, the compound choked points are marked by the symbols on the three performance curves for each mixer.

For primary nozzle pressure ratios greater than or equal to that at which the ejector compound chokes, two ejector exit solutions are possible: 1) Compound supersonic and 2) compound subsonic. (The situation is analogous to a converging–diverging nozzle.) The compound subsonic solution is characterized by a compound shock in the mixing duct and an outflow static pressure that is matched to ambient; the compound supersonic outflow is characterized by an outflow static pressure that is not necessarily matched to ambient. As is the case with converging–diverging nozzles, the nozzle pressure ratio and starting history determine the exit solution that is realized in practice.

In the region of Fig. 12, where all three mixers are operating compound subsonically (NPR < 3.25), pumping and thrust augmentations are associated with the increased interface length offered by the lobed mixer (Γ^* = 0.0) relative to the flat plate. An additional pumping augmentation is associated with the streamwise vorticity shed by the forced mixer. However, in Fig. 12 no additional thrust augmentation is associated with the presence of the streamwise vorticity. For the mixer geometry and run conditions utilized for this trade study, the thrust loss associated with generating the streamwise vorticity just balances the thrust augmentation derived from the vorticity enhanced pumping. (As will be seen in Sec. IV, for $h^* \leq 1.25$, a thrust augmentation is associated with the vorticity shed by the 15-deg forced mixer; for $h^* \geq 1.25$, a thrust penalty is associated with that vorticity.)

Additionally, as may be seen in Fig. 12, the mixers with the higher mixing rate compound choke at a lower NPR because of their increased pumping. Because of the increased noise associated with a compound supersonic outflow and operability problems associated with the movement of the compound shock in the mixing duct, it may not be desirable to operate the ejector in the compound supersonic regime. Hence, for duct geometry and run conditions at which this trade study was conducted, it is possible to mix too rapidly. For example, in Fig. 12, at NPR = 4.0, the flat-plate mixer operates compound subsonically and generates a secondary to primary mass flow ratio of 0.4. At this NPR, the other two mixers would offer increased pumping. However, they would either be operating with a compound supersonic exit or with a compound shock in the mixing duct, both undesirable situations.

V. Impact of Mixer Height and Lobe Angle on Ejector Performance

In the previous section a subset of potential mixer designs (h^* restricted to 1.25) was investigated over a range of operating conditions to illustrate the impact of streamwise vorticity on ejector performance. In this section, a broader range of designs is considered, but at a fixed operating point. Two mixer design parameters are investigated: 1) The mixer height-to-wavelength ratio h^* and 2) the lobe angle α. The mixer lobes

were again of a square lobe design; hence, the vorticity distribution was assumed constant along the vertical side walls of the mixer. Two analyses were conducted. First, the vortex code was utilized to investigate the impact of h^* and α on the mixing rate; this analysis is presented in Sec. V.A. Second, the full system model was exercised to investigate the influence of the two mixer design parameters on ejector pumping and thrust; this study is described in Sec. V.B. The lobe and duct geometries for which these analyses were performed are as follows: A_s/A_p = 1.0, $A_{exit}/A_{in.}$ = 1.0, l_{duct}/λ = 30, h_{duct}/λ = 5, h^* = 0.5–2.75, penetration = 0.1–0.55, and α = 0–25 deg.

A. Impact of Streamwise Vorticity on Mixing Rate

A series of simulations were performed with the vortex model to assess the impact of streamwise vorticity on the mixing rate over the range of lobe heights specified in the preceding text. The shear-layer growth rate and trailing-edge boundary-layer thickness utilized for the simulations were 0.125 and 0.25, respectively. These values are typical of those for the experiments discussed in Sec. III.

In Fig. 13 the scalar mixedness at the mixing duct exit is plotted vs h^* and α. A mixing benefit resulting from the stretching of the crossflow interface is associated with streamwise vorticity at all lobe heights investigated. In Fig. 14 the scalar mixing augmentation associated with streamwise vorticity at the duct exit is plotted vs h^* and α. The scalar mixing augmentation at a distance x^* from the mixer is given by

$$\Delta M_{sc}(x^*) = \frac{M_{sc}(x^*)|_{\Gamma} - M_{sc}(x^*)|_{\Gamma=0}}{M_{sc}(x^*)|_{\Gamma=0}} \tag{9}$$

where $\Delta M_{sc}(x^*)$ is the normalized increase in scalar mixedness associated with the streamwise vorticity. As may be seen in Fig. 14 the effectiveness of the vorticity decreases with increasing lobe height-to-wavelength ratio.

The reason for the decreased effectiveness is illustrated in Fig. 15, where the scalar fields 2λ downstream of four 15-deg forced mixers with height-to-wavelength ratios of 0.5, 1.25, 2.00, and 2.75 are shown. As h^* increases, the rate of stretching of the interface decreases. Hence, the vorticity is less effective in increasing the mixing rate. The mechanism for the decreased mixing rate with increasing h^* is related to the effect described in Sec. III.B, where a higher diffusion rate led to a decreased effectiveness of Γ^*. In the current situation, closer proximity of vorticity of the opposite sign from neighboring lobes leads to decreased effectiveness of Γ^*; the decreased effectiveness is because of the more rapid cancellation of the vorticity by diffusion between adjacent lobes.

B. Impact of Streamwise Vorticity on Ejector Pumping and Thrust

The full mixer–ejector model was then utilized to investigate the impact of streamwise vorticity on the pumping and thrust of an ejector. The flow conditions and geometric parameters for which the trade study was conducted are tabulated next: NPR = 3.0, SNPR = 1.0, M_p = 1.6, Tt_p/Tt_s = 3.0, mixer C_t = 0, and duct C_f = 0.

In Figs. 16 and 17, the predicted pumping and gross thrust coefficients are plotted, respectively, vs lobe angle for mixers with h^* = 0.5, 1.25, 2.00, and 2.75.

Recall that in Figs. 13 and 14 it was demonstrated that a mixing augmentation is associated with the generation of streamwise vorticity at all lobe heights. However, as shown in Figs. 16 and 17, an ejector performance trade associated with the generation of the vorticity is evident. The streamwise vorticity enhances the mixing rate downstream of the mixers. The enhanced mixing rate tends to increase the pumping and thrust performance of the ejector. However, a mixer drag penalty caused by the generation of the vorticity tends to reduce the pumping and thrust of the ejector.

Furthermore, in Figs. 13–15, streamwise vorticity is seen to be less effective in augmenting the mixing rate with increasing h^*. A near 35% increase in the mixedness at the duct exit was found for a Γ^* of 0.9 (α = 25 deg) for a mixer with h^* = 0.5; however, only a 7% increase was calculated for Γ^* = 0.9 for a mixer with h^* = 2.75. Furthermore, as h^* is increased at a

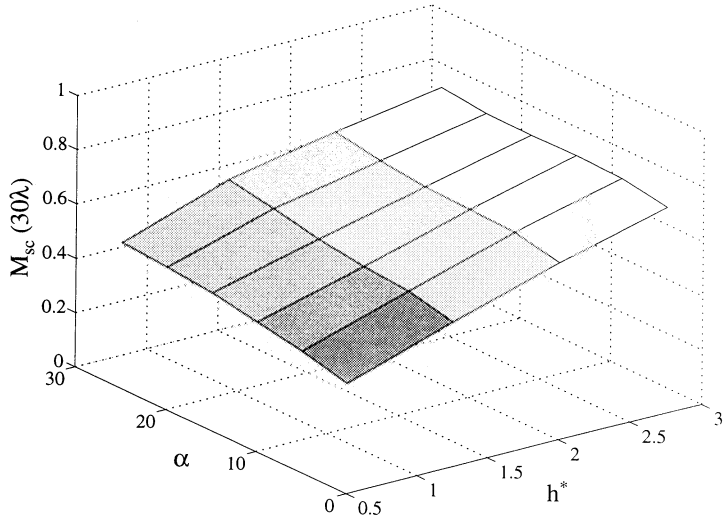

Fig. 13 Scalar mixedness at the duct exit (30λ) vs h^* and α (δ'_{vel} = 0.10 and ε^* = 0.25).

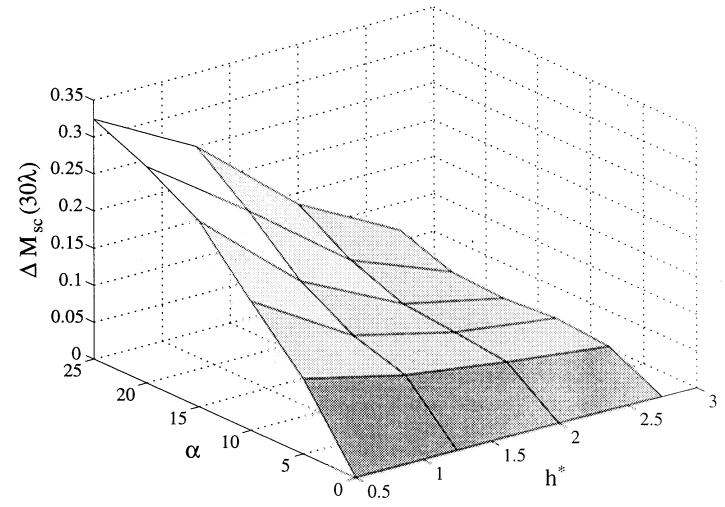

Fig. 14 Scalar mixing augmentation at the duct exit (30λ) vs h^* and α (δ'_{vel} = 0.10 and ε^* = 0.25).

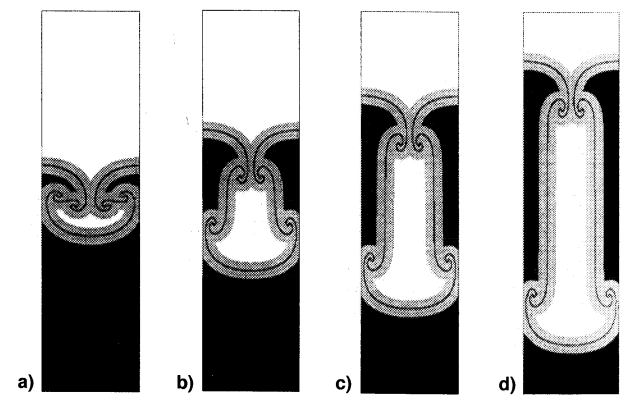

Fig. 15 Scalar fields 2λ downstream of 15-deg forced mixers at four different lobe height-to-wavelength ratios (δ'_{vel} = 0.10 and ε^* = 0.25). h^* = a) 0.5, b) 1.25, c) 2.00, and d) 2.75.

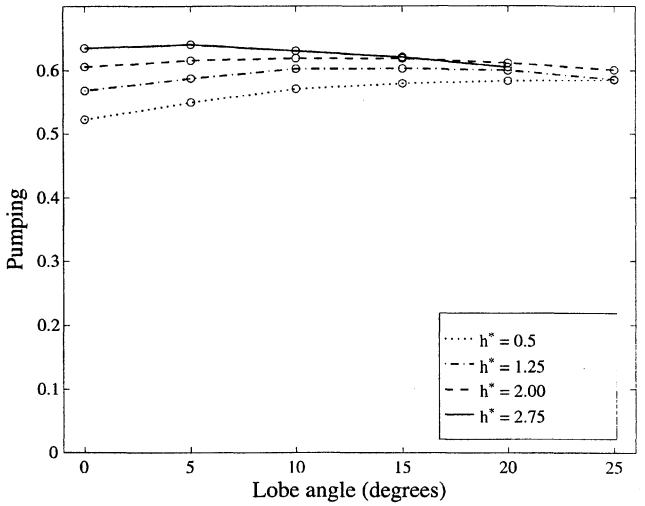

Fig. 16 Predicted entrained/primary mass flow ratio vs lobe angle for NPR = 3.0, SNPR = 1.0, A_s/A_p = 1.0, and Tt_p/Tt_s = 3.0.

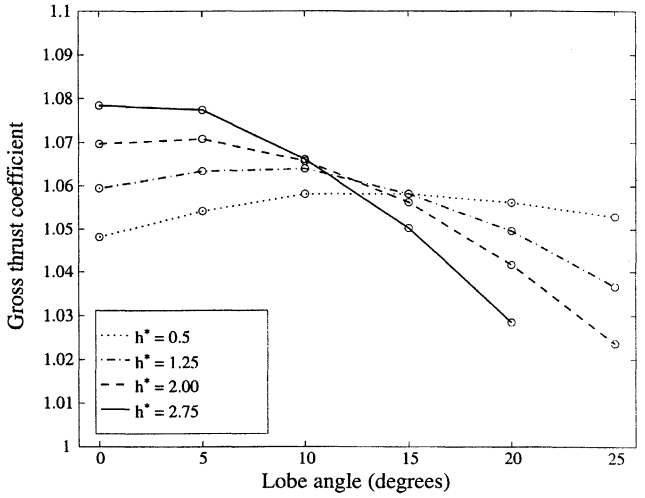

Fig. 17 Predicted gross thrust coefficient vs lobe angle for NPR = 3.0, SNPR = 1.0, A_s/A_p = 1.0, and Tt_p/Tt_s = 3.0.

constant lobe angle, the penetration of the mixer increases and, hence, the fraction of the duct inflow vectored off-axis increases.

As is evident in Figs. 16 and 17, the pumping and thrust penalties associated with the generation the streamwise vorticity at high h^* and high penetration outweigh the mixing benefit of the vorticity. At $h^* = 2.75$, a 2% drop in pumping and an 3% drop in gross thrust coefficient are associated with vectoring the inflow through a 15-deg angle and generating $\Gamma^* = 0.5$. On the other hand, at $h^* = 0.5$ a 12% increase in pumping and a 1% increase in C_{TG} are found for $\Gamma^* = 0.5$.

Of the mixer geometries evaluated, $h^* = 2.75$ the mixer with the highest pumping and thrust was the mixer that shed no streamwise vorticity. Hence, the results of this study indicate that to maximize both the thrust and pumping of a mixer–ejector, one should design a mixer that maximizes the initial interfacial area between the streams and minimizes the streamwise vorticity shed. However, no skin friction model was utilized in this comparison, and mixer skin friction will tend to degrade the performance of the higher h^* mixers relative to the smaller h^* mixers. Additionally, in an actual mixer–ejector, it may be difficult to design a mixer of acceptable length and weight that sheds little streamwise vorticity. The straight section of the convoluted plate mixer ($\Gamma^* = 0.03$) evaluated in the experiments was over 1.25 lobe heights in length. A longer straight section would generate less streamwise vorticity, and a shorter straight section would generate more vorticity. If a shorter mixer is desired, it may be more effective to use a geometry with a lower h^*.

VI. Summary and Conclusions

A mixer–ejector model has been developed to predict the pumping and thrust of mixer–ejector noise suppressors. This model is flexible and efficient relative to current computational performance prediction techniques; it runs 100 times faster than three-dimensional Navier–Stokes computations, and no grid generation is required.

The model was described and sensitivity studies were conducted with each component to illustrate the influence of key mixer–ejector design parameters. Comparisons were also made to experimental data, including Mie scattering images, wall static pressures, and mass flow measurements. The model qualitatively captured the evolution of the mixing interface with distance from the trailing edge of the mixer, and produced quantitative estimates of the change in pressure coefficient through the duct to within 15% of the measured values over a range of mixer geometries and operating conditions. Additionally, two design trade studies were presented in which the model was used to assess the impact of streamwise vorticity on mixer–ejector performance.

The results of sensitivity and design trade studies have elucidated several important mixer–ejector design considerations:

1) Opposing trends in the form and skin friction drag coefficients with varying lobe angles result in a minimum in the drag coefficient vs lobe angle curve.

2) The effectiveness of streamwise vorticity decreases with an increasing shear-layer growth rate.

3) Because it is often desirable to operate mixer–ejectors compound subsonically, it is possible to mix the two streams of fluid too rapidly, for low secondary-to-primary area ratio ejectors.

4) A pumping, but not a thrust, augmentation has been associated with the streamwise vorticity shed by a 15-deg forced mixer with a height-to-wavelength ratio of 1.25.

5) The effectiveness of streamwise vorticity decreases with an increasing mixer height-to-wavelength ratio and with increasing shear-layer growth rate.

Hence, for the higher height-to-wavelength ratios investigated, the performance penalties associated with generating the streamwise vorticity are larger than the performance augmentation associated with the increased mixing rates. However, in a practical device, because of the length of the straight section required to turn the flow axially, it may not be possible to design a mixer that sheds no vorticity; hence, it may be better to utilize a mixer with a smaller h^*, but larger lobe angle.

Acknowledgments

Support for this work was provided by NASA Langley Research Center under NASA Grant NAG-1-1511 with Jack Seiner as the Technical Monitor, and under NASA Contract NAS3-27235, Subcontract PO F760652 to Pratt and Whitney with Edwin Kawecki as the Technical Monitor. This support is gratefully acknowledged. The authors also thank Edward Greitzer, Choon Tan, Frank Marble, James Hermanson, and Frank Zumpano for their consultations and insightful suggestions during the course of this work.

References

[1]Waitz, I. A., Qiu, Y. J., Elliott, J. K., Fung, A. K. S., Kerwin, J. M., Krasnodebski, J. K., O'Sullivan, M. N., Tew, D. E., Greitzer, E. M., Marble, F. E., Tan, C. S., and Tillman, T. G., "Streamwise Vorticity Enhanced Mixing," *Progress in Aerospace Sciences*, Vol. 33, No. 5–6, 1997, pp. 323–351.

[2]Elliott, J. K., "A Computational Investigation of the Fluid Dynamics of a Three-Dimensional Compressible Mixing Layer with Strong Streamwise Vorticity," M.S. Thesis, Massachusetts Inst. of Technology, Cambridge, MA, 1990.

[3]Qiu, Y. J., "A Study of Streamwise Vorticity Enhanced Mixing in Lobed Mixer Devices," Ph.D. Dissertation, Massachusetts Inst. of Technology, Cambridge, MA, 1992.

[4]Manning, T. A., "Experimental Studies of Mixing Flows with Streamwise Vorticity," M.S. Thesis, Massachusetts Inst. of Technology, Cambridge, MA, 1991.

[5]Barber, T., Paterson, R. W., and Skebe, S. A., "Turbofan Forced Mixer Lobe Flow Modeling," NASA CR-4147, Oct. 1988.

[6]O'Sullivan, M. N., Waitz, I. A., Greitzer, E. M., Tan, C. S., and Dawes, W. N., "Computational Study of Viscous Effects on Lobed Mixer Flow Features and Performance," *Journal of Propulsion and Power*, Vol. 12, No. 3, 1996, pp. 449–456.

[7]Papamoschou, D., and Roshko, A., "The Compressible Turbulent Shear Layer: An Experimental Study," *Journal of Fluid Mechanics*, Vol. 197, 1988, pp. 453–477.

[8]Tew, D. E., "A Computational Study of Mixing Downstream of a Lobed Mixer with a Velocity Difference Between the Co-Flowing Streams," M.S. Thesis, Massachusetts Inst. of Technology, Cambridge, MA, 1992.

[9]Clark, L. T., "Application of Compound Flow Analysis to Supersonic Ejector-Mixer Performance Prediction," AIAA Paper 95-0645, Jan. 1995.

[10]Tew, D. E., "Streamwise Vorticity Enhanced Compressible Mixing Downstream of Lobed Mixers," Ph.D. Dissertation, Massachusetts Inst. of Technology, Cambridge, MA, 1997.

[11]Tew, D. E., Waitz, I. A., Hermanson, J. C., Greitzer, E. M., and Tan, C. S., "Streamwise Vorticity Enhanced Compressible Mixing Downstream of Lobed Mixers," AIAA Paper 95-2746, July 1995.